ACS Sustainable Chemistry & Engineering

pubs.acs.org/journal/ascecg

Research Article

Co(salen)-Catalyzed Oxidation of Lignin Models to Form Benzoquinones and Benzaldehydes: A Computational and Experimental Study

Connor J. Cooper, Shahrina Alam, Vincent de Paul N. Nziko, Ryne C. Johnston, Alexander S. Ivanov, Zhongyu Mou, David B. Turpin, Alan W. Rudie, Thomas J. Elder, Joseph J. Bozell,* and Jerry M. Parks*

Cite This: https://dx.doi.org/10.1021/acssuschemeng.0c01970

Read Online

ACCESS | Metrics & More | Article Recommendations | Supporting Information

ABSTRACT: Lignin is a highly abundant polyphenolic polymer that imparts mechanical strength to plant biomass. Transition-metal complexes can catalyze lignin oxidation to produce value-added products, but low catalytic efficiency has hampered their use in industry. Identifying the chemical and structural factors that govern catalytic activity is a prerequisite to rational design of catalysts with improved activity. Here, we combine computational and experimental approaches to investigate the mechanism of Co(salen)-catalyzed oxidation of the monomeric lignin models syringyl (S), vanillyl (G), and 4-hydroxybenzyl alcohol (H) to produce benzoquinone and benzaldehyde products. Experimentally, S oxidation to form dimethoxybenzoquinone proceeded efficiently with a Co(salen) catalyst coordinated by a pyridine ligand, but G and H did not undergo oxidation. Density functional theory calculations reveal that catalyst regeneration is energetically unfavorable in the presence of H, which prevents oxidation. In contrast, S readily facilitates catalyst regeneration. Formation of methoxybenzoquinone from G was achieved experimentally by adding bulky, noncoordinating bases. These findings provide a fundamental baseline for enhancing the activity of Co-Schiff base catalysts toward lignin-like molecules by adding sterically hindered nitrogenous bases or potentially by including a cocatalyst that promotes catalyst regeneration.

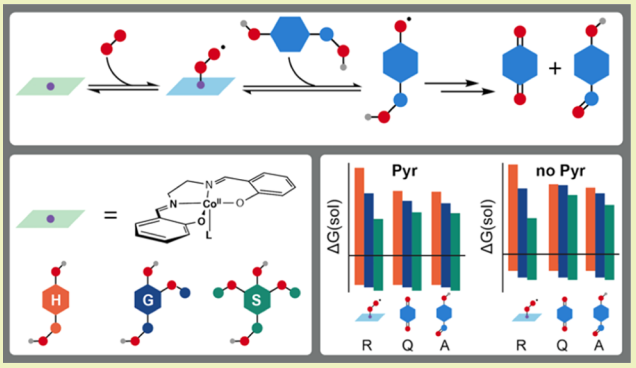

KEYWORDS: *Schiff base, valorization, biomass, transition metal, density functional theory, catalysis*

INTRODUCTION

The integrated biorefinery has emerged as an alternative to the petrochemical refinery for the simultaneous production of biobased chemicals and fuels. Critical to the emergence of a sustainable industry based on biomass is the ability to use all components of the raw material in high-value applications. Biorefining offers selective access to each of the primary constituents of lignocellulosic biomass, with biobased carbohydrates offering multiple opportunities for further conversion to chemicals and fuels.[1,2] In contrast, the lignin component presents particular challenges. As much as 30% of biomass is lignin, making it the second most abundant source of renewable carbon in the biosphere.[3−5] "Lignin valorization" for the selective production of chemicals is of great interest for biorefinery development.[6−14] However, lignin possesses a highly heterogeneous assembly of multiple substructural units (Figure 1A) resulting from coupling of delocalized phenoxy radicals during biosynthesis.[15,16] Lignin from woody feedstocks is constructed mostly from syringyl (S) and guaiacyl (G) units derived from sinapyl and coniferyl alcohol, respectively. Herbaceous feedstocks (grasses) incorporate additional *p*-

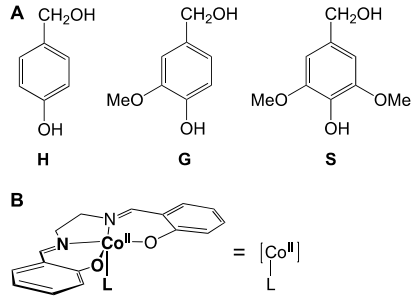

Figure 1. (A) Syringyl (S), guaiacyl (G), and *p*-hydroxyphenyl (H) lignin models. (B) Co(salen) catalyst and L = methanol or pyridine.

Received: March 11, 2020
Revised: April 7, 2020
Published: April 17, 2020

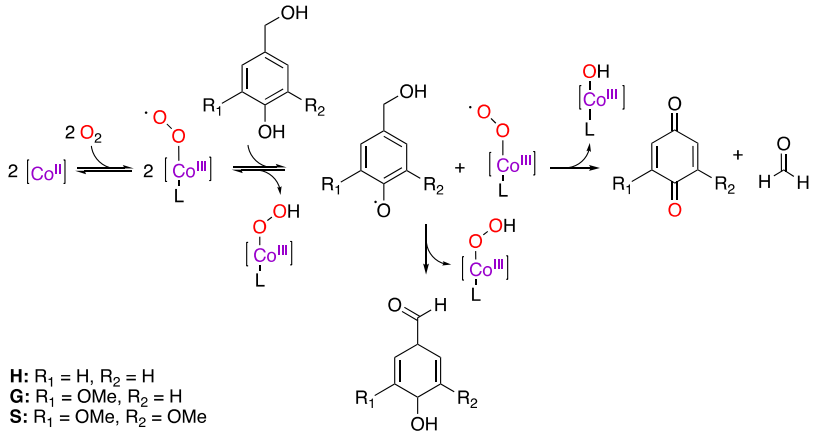

Figure 2. Generally accepted mechanism of Co(salen)-catalyzed oxidation of lignin-like phenols to form quinones and aldehydes.

hydroxyphenyl (H) units into the lignin polymer as well as coumaric and ferulic acid as end caps and crosslinkers.[17] Moreover, when lignin is isolated during biorefining, its structure changes further, and often dramatically, as a result of the processes used to separate lignin from the carbohydrate components of biomass.[18] Because of these challenges, lignin is often relegated to be used as a process fuel in biorefinery operations, which is an ineffective use of this sustainable source of aromatic carbon. The most sustainable use of lignin as a chemical feedstock therefore requires processes that are able to adapt to its wide range of inherent structural units either in native lignin ("lignin-first" conversions) or as isolated during biomass processing.

To address this challenge, a recent report describes the development of catalytic systems tailored for lignin deconstruction and conversion to higher value materials.[19] Active research in homogeneous transition metal catalysis has identified promising candidates for oxidative lignin degradation.[4,12,20−22] Methods for transforming lignin models into low molecular weight aromatics have been carried out using reductive processes catalyzed by Ru,[23,24] Ni,[25,26] and Pd,[27] oxidative and nonoxidative processes catalyzed by Co[4] and V,[28,29] or organocatalytic processes using 2,2,6,6-tetramethylpiperidine-*N*-oxyl.[30]

Of particular interest for lignin conversion are Co-Schiff base species such as Co(salen), that is, [*N*,*N*′-bis-(salicylidene)-ethane-1,2-diaminato]cobalt (Figure 1B), which has been used to catalyze the oxidation of phenols.[31−35] Co-Schiff base catalysts operate under mild conditions, use plentiful O_2 and nonprecious transition metals, and produce valuable chemical feedstocks as byproducts. The resulting oxidized products include high-value chemicals such as quinones and aldehydes, which can be repurposed. However, low turnover numbers, low selectivity for lignin over polysaccharides, or both have hampered their use in larger-scale operations.

The generally accepted mechanism of Co-Schiff base-catalyzed oxidation involves activation of O_2 to form a Co^{III}−superoxide adduct (Figure 2).[33] The Co^{III}−superoxo adduct then removes a phenolic hydrogen from the substrate to form a phenoxy radical, which reacts with a second equivalent of the Co^{III}−superoxo adduct to form a peroxo intermediate that undergoes subsequent rearrangement to form quinones, aldehydes, or both. The presence of an axial ligand, such as pyridine, has been shown to facilitate Co^{III}−superoxide formation.[36] Notably, both Co^{III}−hydroxo and Co^{III}−hydroperoxo intermediates are formed during these reactions.

Previously proposed mechanisms for the oxidation of phenols by Co-Schiff base catalysts include the formation of Co^{III}−hydroxide and Co^{III}−hydroperoxide adducts.[32,33] A mechanism was proposed for catalyst regeneration from the resulting L−Co^{III}−OH intermediate in a related Co-Schiff base system in which a phenolic hydrogen atom is transferred to the hydroxy group to form H_2O, which then dissociates to regenerate the catalytically active Co^{II} complex.[33] More recently, the mechanism of aerobic oxidation of *p*-hydroquinone by Co(salophen) to form *p*-benzoquinone was examined using a combination of experimental kinetics, spectroscopy, and density functional theory (DFT) calculations.[37] The turnover-limiting step was identified as a proton-coupled electron transfer between a semiquinone and Co^{III}−hydroperoxo intermediate to oxidize one equivalent of *p*-hydroquinone (Figure 3). Subsequently, a coordinated H_2O_2 intermediate was found to oxidize the second equivalent of *p*-hydroquinone and regenerate the catalyst.

The study of the mechanism of aerobic oxidation of *p*-hydroquinone[37] is important for our purposes for two reasons: first, it provides an informative starting point for identifying plausible catalyst regeneration pathways involving lignin

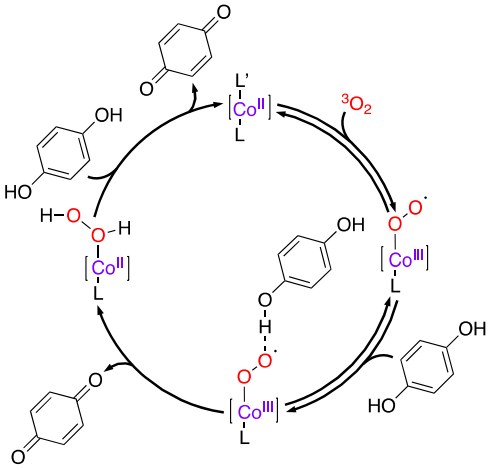

Figure 3. Proposed mechanism for the Co(salophen)-catalyzed aerobic oxidation of *p*-hydroquinone to form benzoquinone from ref 37.

https://dx.doi.org/10.1021/acssuschemeng.0c01970
ACS Sustainable Chem. Eng. XXXX, XXX, XXX−XXX

models. Second, it provides an experimentally validated DFT-based approach for describing oxidation reactions catalyzed by a Co(salen) catalyst. Noted differences between the two systems are our use of salophen in the present work as opposed to salophen, and our use of H, G, and S models, which are benzylic phenols bearing up to two methoxy groups, instead of *p*-hydroquinone. However, it has been shown that Co-(salophen) with a pyridine ligand catalyzes the oxidation of the S model to form dimethoxybenzoquinone (DMBQ) with a yield of 100%, essentially identical to the analogous reaction with Co(salen).[38] In addition, in terms of chemical reactivity we note that *p*-hydroquinone is intrinsically much easier to oxidize to quinone than the H, G, and S models.

A prerequisite to designing catalysts with improved activity is the identification of chemical and structural factors that govern catalytic activity. Here, we have performed complementary experiments and DFT calculations to investigate the mechanism of Co(salen)-catalyzed oxidation of monomeric lignin models to form benzoquinones and benzaldehydes. Experimentally, oxidation of the S model to form DMBQ proceeded efficiently with pyridine-ligated Co(salen), but G and H were not oxidized. We calculated reaction pathways for catalyst regeneration and show that these steps are critical for facilitating sustained turnover. Though catalyst regeneration occurs readily in the presence of S, it cannot occur with H because of unfavorable energetics. The calculations also suggest that benzaldehyde formation may be more limited by catalyst regeneration bottlenecks than benzoquinone formation.

METHODS

Computational. All calculations were performed using a previously described quantum chemical method that was shown to provide an accurate description of *N*,*N*′-disalicylidene-ethylenediamine cobalt(II), that is Co^{II}(salophen), catalyst system,[37] which is very similar to the Co(salen) system investigated here. Briefly, we used the M06-L[39] density functional approximation with the LANL2DZ effective core potential and basis set for Co,[40] the 6-31G(d,p) basis set with 5D functions[41−43] for all other elements. The solvation model density polarizable solvent model[44] with methanol as the solvent was used to calculate molar solution-phase free energies. For $^3O_2$ only, the gas-phase free energy was used, and a standard state correction was added to the gas-phase value to account for the change in concentration of 1 atm to 1 M, that is, $\Delta G^{\circ\rightarrow *} = RT\ln(24.5) = +1.89$ kcal/mol. Vibrational frequencies were calculated to confirm the absence of imaginary frequencies for each minimum-energy state and the presence of a single imaginary frequency corresponding to the reaction of interest for each transition state. All calculations were performed with Gaussian 16 rev A.03.[45] To generate the reaction free energy diagrams, various species were added as needed to maintain the correct stoichiometry at each step. All optimized geometries and their corresponding total energies are provided in Supporting Information.

Experimental Section. *General Procedure for the Oxidation of Lignin Models.* CAUTION: The oxidation reactions were performed in thick-walled, glass Fisher−Porter tubes under pressurized oxygen. Though no difficulties were experienced, adequate precautions should be considered when using organic compounds and oxygen above atmospheric pressure. Lignin models were oxidized according to a previously published procedure.[31,34] Briefly, to a Fisher−Porter tube were added 1 equivalent of the lignin model, 0.1 equivalents of Co(salen) catalyst, and the appropriate amount of methanol to make a 0.2 M solution relative to the lignin model substrate. The tube was flushed three times and then pressurized to 60 psi using oxygen. Once pressurized, the reaction was stirred at room temperature for times denoted in Tables 1−4. The entire reaction mixture was then transferred to a round-bottom flask using dichloromethane. The solvent was removed on the rotary evaporator at 30 °C, and the residue was dried overnight under vacuum. After drying, the sample was dissolved in 100 mL of acetonitrile using a volumetric flask.

Table 1. Formation of Benzoquinones or Benzaldldehydes from Lignin Models in the Presence of Co(salen)

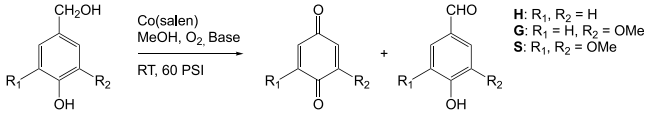

substrate	base	reaction time (h)	quinone yield (%)	aldehyde yield (%)
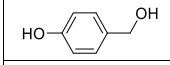		22	0	0
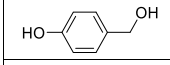	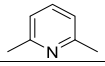	22	0	0
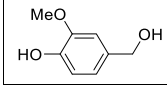		22	0	0
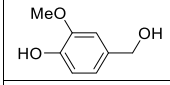		22	0	0
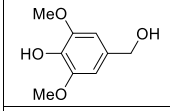		1	99	0
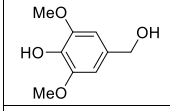		1 22	52 58	26 15
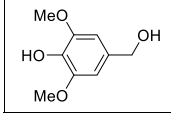	none	1 22	36 41	23 8

Table 2. Formation of MBQ from a G Lignin Model in the Presence of a Bulky, Noncoordinating Base[a]

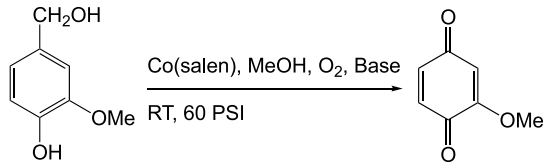

base added	pK_{BH}^+	MBQ yield (%)
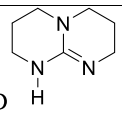 TBD	25.98 (MeCN)	38
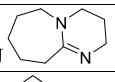 DBU	24.33 (MeCN)	59
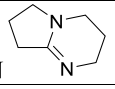 DBN	23.89 (MeCN)	30
DIPEA [EtN(i-Pr)2]	11.05 (water)	68
 DABCO	8.4 (water)	0

[a]All reactions were carried out for 22 h.

https://dx.doi.org/10.1021/acssuschemeng.0c01970
ACS Sustainable Chem. Eng. XXXX, XXX, XXX−XXX

Table 3. Formation of DMBQ from Syringaldehyde

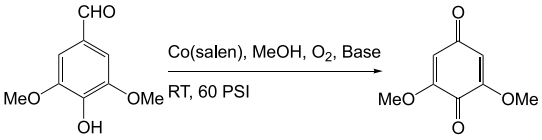

catalyst	base added	reaction time (h)	DMBQ yield (%)
none		1	0
none	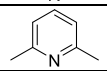	1	0
Co(salen)		1	3
Co(salen)	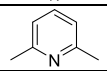	1	26
Co(salen)	none	1	26
		22	94

Table 4. Formation of Benzaldehyde from 3,4,5-Trimethoxybenzyl Alcohol

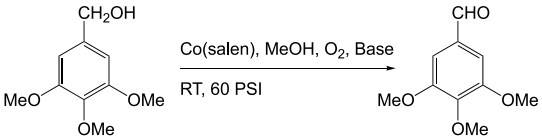

base added	reaction time (h)	benzaldehyde yield (%)
	1	8
	22	9
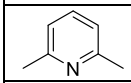	1	5
NaOH	22	2
	80	87 (carboxylic acid)
none	1	4
	22	5
	22	6

Aliquot of the solution (5 mL) was dissolved in 100 mL of 25:75 MeCN/H_2O. The resulting mixture was analyzed by high-performance liquid chromatography (HPLC). HPLC analysis was carried out using a Waters model 2695 separations module, a Waters model 2996 photodiode array detector, and a 100 Å, 3.5 μm, 3 mm × 150 mm SunFire C18 column. Yields were determined from calibration curves measured for each product and adjusted for the appropriate dilution factor.

RESULTS AND DISCUSSION

To provide insights into the mechanisms of lignin oxidation by the Co(salen) catalyst, we used DFT to calculate reaction pathways for the formation of quinones and aldehydes from the corresponding syringyl alcohol (S), vanillyl alcohol (G), and *para*-hydroxybenzyl alcohol (H) lignin models (Figure 1A). The active form of the catalyst must be regenerated during the course of the reaction to achieve sustained turnover. Therefore, we first considered catalyst regeneration steps analogous to those previously described for *p*-hydroquinone oxidation.[37] In that pathway, two equivalents of *p*-hydroquinone are converted to two equivalents of *p*-benzoquinone per equivalent of O_2, that is, both phenolic OH groups undergo oxidation (Figure 3). However, lignin-like phenols contain only a single phenolic group and a para substituent, which is important because both hydroquinone and unsubstituted phenols undergo Co-catalyzed oxidation more easily than para-substituted phenolics. Thus, in the present case, catalyst regeneration is expected to require four equivalents of a given lignin-like phenol per molecule of O_2 instead of two. We generated complete reaction free energy diagrams for catalyst regeneration steps of S, G, and H lignin models both with and without a pyridine ligand (Figures 4 and S1).

Catalyst Regeneration. Oxidation of the lignin models begins with binding of O_2 to Co^{II}(salen) to form Co^{III}–superoxo adduct **2**. This step was calculated to be energetically downhill by 5.0 kcal/mol in the presence of pyridine, which is consistent with the observed weak binding of O_2 to Co(salen).[46] Addition of pyridine as a ligand to Co substantially enhances the favorability of superoxo adduct formation.[47] However, the increased favorability of Co^{III}–superoxo adduct formation afforded by the pyridine ligand to Co results in a slight net increase in the overall free energy barrier for quinone and aldehyde formation.

Association of each lignin model to form intermediate **3** is further downhill energetically relative to reactants and follows the pattern that **3** is most favorable for the S model (−9.5 kcal/mol), followed by the G model (−8.6 kcal/mol) and, finally, the least favorable H model (−7.5 kcal/mol). Abstraction of the phenolic hydrogen from each lignin model by the Co^{III}–superoxo adduct proceeds through **3-TS** to form complex **4**, which consists of a phenolic radical and a Co^{III}–hydroperoxo adduct. Hydrogen atom removal from the S models has a markedly lower energy requirement than removal from H or G models (Scheme S1). The resulting phenolic radical can then enter either the benzoquinone or benzaldehyde pathway at various points (see below).

The catalyst regeneration pathway is required upon formation of the Co^{III}–hydroperoxo species in **4**. The nascent phenolic radical departs and is replaced by a second equivalent of the S, G, or H lignin models to form **5** (Figure 4). The phenolic hydrogen is then abstracted by the proximal oxygen of the Co^{III}–hydroperoxo species through a proton-coupled electron transfer step, resulting in the formation of Co^{II}(salen) with a loosely coordinated H_2O_2 axial ligand, **6**, via **5-TS**. Replacement of the resulting phenolic radical with another equivalent of phenol, along with incorporation of methanol into a hydrogen bond network, generates intermediate **7**. H_2O_2 then undergoes homolysis through **7-TS** to generate a hydroxyl radical and a Co^{III}–hydroxo species in **8**. The phenolic hydrogen from a third equivalent of S, G, or H is transferred to the hydroxyl radical to form H_2O and another phenolic radical in **9**. All steps from **9** onward are lower in free energy than the reactants, indicating their favorability. The phenolic radicals generated throughout the regeneration pathway in **4**, **6**, **9**, and **12** can feed back asynchronously into the quinone and aldehyde pathways discussed below.

The calculations indicate that transition state **7-TS** is the highest-energy state of the regeneration pathway for all three lignin models. In energetic terms, the most stable intermediate in all pathways for all three lignin models is **3**, which sets the energetic baseline for determining the activation barrier for each reaction step. The activation barrier is the lowest for the S

https://dx.doi.org/10.1021/acssuschemeng.0c01970
ACS Sustainable Chem. Eng. XXXX, XXX, XXX−XXX

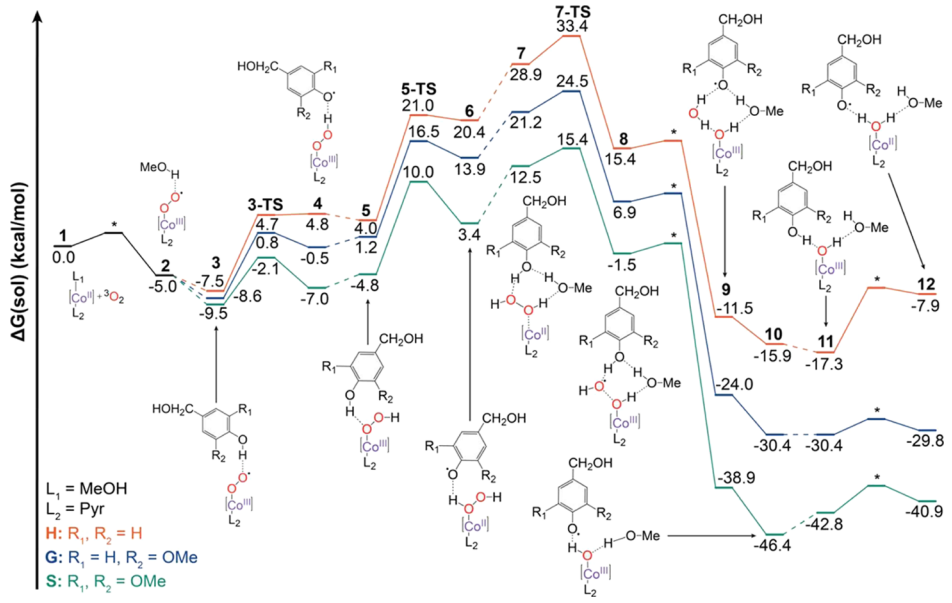

Figure 4. Free energy diagram for the initial formation of the active Co^{III}–superoxo catalyst with an axial pyridine ligand and subsequent catalyst regeneration during oxidation of S, G, and H lignin models. Phenolic radicals generated at **4**, **6**, **9**, and **12** can feed into the quinone and aldehyde pathways described below. Dashed lines indicate the introduction of an additional equivalent of the S, G, or H lignin models, and asterisks indicate transition states that were not calculated.

model (24.9 kcal/mol). This barrier is higher in energy for the G model (33.1 kcal/mol), and the H model is the least favorable (40.9 kcal/mol). These findings are consistent with previous work in which it was reported that S models underwent facile oxidation, whereas G models did not.[34] Furthermore, it was shown that the rates of reaction for hydrogen atom removal from phenols follows the same trend (i.e., S > G > H).[48]

We also calculated free energy diagrams for the catalyst regeneration pathways without a pyridine ligand to Co (Figure S1). The energy difference between the lowest energy step **3** and **7-TS** is the lowest for the S model (21.9 kcal/mol). This reaction for the G model is less favorable (31.4 kcal/mol) followed by the H model (37.5 kcal/mol). Without pyridine, the formation of the Co^{III}–superoxo adduct is 3.5–4.7 kcal/mol less favorable than when pyridine is included (Figures 4 and S1). The absence of an axial base results in a reduced impact on the d_{z^2} orbital on the Co, that is, its energy is not raised as much, whereas the presence of a Co-axial base interaction raises the energy of the d_{z^2} orbital so that it can bind effectively to O_2.[47,49] Thus, although the free energies for **7-TS** are slightly higher in the absence of pyridine, the overall barriers in the presence of pyridine are higher because pyridine coordination lowers the energy of **3** relative to reactants.

Benzoquinone Formation. The mechanism of benzoquinone formation is identical to that of the catalyst regeneration pathway through **4**. For the catalytic cycle to continue, the Co^{III}–hydroperoxo species generated at this step must be converted back to the Co^{III}–superoxo state or it must be replaced by a second equivalent of the Co^{III}–superoxo adduct to generate **13** (Figure 5). At early stages of the reaction, we expect that the Co^{III}–superoxo adduct will be present in abundance because its formation from Co^{II}(salen) and O_2 is energetically favorable. Thus, for this mechanism, we assume that a Co^{III}–superoxo species is available to enable formation of **14** from diradical species **13**.

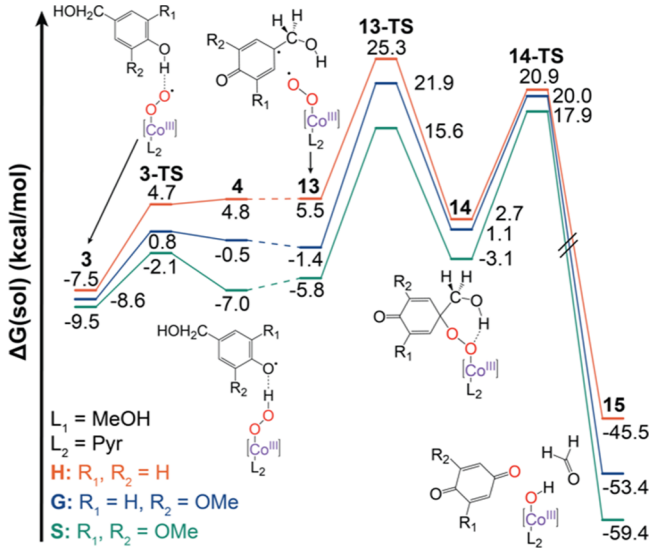

Figure 5. Free energy profile for the catalytic oxidation of lignin model compounds by Co(salen) with an axial pyridine ligand to form benzoquinones. Energies are relative to **1**. Note that the inactivated Co^{III}–hydroperoxo species in **4** must be replaced by a second equivalent of the Co^{III}–superoxo complex to generate **13** and enable turnover. Dashed lines indicate the introduction of another equivalent of active catalyst.

Coupling of the Co^{III}–superoxo adduct with a phenolic radical then proceeds through **13-TS** to form covalent adduct **14** (Figure 5). This species then decomposes via **14-TS** to produce formaldehyde, a catalytically inactive Co^{III}–hydroxo adduct, and the benzoquinone product. The Co^{III}–hydroxo adduct can then undergo facile regeneration analogous to **11** (Figure 4). Either **13-TS** or **14-TS** is rate-limiting, depending on the substrate and the presence/absence of a pyridine ligand. **13-TS** is slightly higher (1.9 kcal/mol) in free energy than **14-TS** for the G model in the pyridine-containing species and

https://dx.doi.org/10.1021/acssuschemeng.0c01970
ACS Sustainable Chem. Eng. XXXX, XXX, XXX−XXX

substantially lower (4.3 kcal/mol) when pyridine is absent, whereas for S, the highest-energy state is **14-TS** in both systems,.

The pathway leading to benzoquinone formation results in the formation of both a Co^{III}–hydroperoxo and Co^{III}–hydroxo adducts (Figure 5). The inactive Co^{III}–hydroxo adduct in **15** can be easily regenerated by bypassing **7-TS** and entering the regeneration pathway at any point between **9** and **11** (Figure 4). However, the Co^{III}–hydroperoxo adduct must proceed from **4** to **5** in the regeneration pathway, passing through the energetically unfavorable **7-TS**.

To provide an experimental baseline for the quinone formation mechanism, we performed a designed set of Co(salen)-catalyzed oxidations of S, G, and H lignin models. Syringyl alcohol was converted to DMBQ in 99% yield after 1 h of oxidation when treated with 10% Co(salen) in methanol in the presence of pyridine under 60 psi of O_2 (Table 1). In contrast, we observed no formation of the (substituted) benzoquinone product when vanillyl alcohol or 4-hydroxybenzyl alcohol were subjected to the same reaction conditions, or alternatively, at an extended reaction time of 22 h. The calculated free energy barrier for H quinone formation with pyridine is 32.8 kcal/mol (Figure 5), but the barrier for catalyst regeneration is 40.9 kcal/mol (Figure 4). As a result, the inability of the H model to facilitate catalyst regeneration appears to prevent oxidation, in agreement with the experimental observations. In contrast, the calculated free energy barrier for DMBQ formation from S is 27.4 kcal/mol with pyridine and the regeneration barrier is 24.9 kcal/mol. The much lower overall free energy barrier for oxidation of the S model is consistent with the nearly quantitative conversion to DMBQ observed experimentally (Table 1).

Role of the Axial Ligand in Quinone Formation. To investigate the role of the axial ligand during the oxidation, we carried out additional oxidation reactions of syringyl alcohol without any added base or alternatively, in the presence of 2,6-lutidine. In the absence of a base, the yield of DMBQ was 36% after 1 h of reaction and 41% at 22 h (Table 1). In this case, we hypothesize that the MeOH solvent serves as a weak axial ligand to Co. When lutidine was used, the yield of DMBQ improved to 52% after 1 h and 58% after 22 h. These results are consistent with a steric effect, in which the approach of the base to Co is hindered by the presence of the methyl groups flanking the pyridine nitrogen.

Effect of Non-Coordinating Bases on Quinone Formation. Previous work has suggested that the use of imidazole-based axial ligands that coordinate to the central Co atom can improve DMBQ yield from the S lignin model.[47] The 99% DMBQ yield we observed experimentally when pyridine was added to the system (Table 1) is consistent with those findings. In agreement with previous results,[49] we did not observe MBQ formation with the G lignin model, even when pyridine was added. In related work, oxidation of G models was observed upon addition of noncoordinating, sterically hindered nitrogenous bases.[32] Considering these observations, we added a series of five bulky, noncoordinating bases to the reaction mixture as a means to promote oxidation of the unreactive G lignin model. We observed measurable yields of MBQ in the presence of most bases (Table 2). 1,5-Diazabicyclo[4.3.0]non-5-ene (DBN), 1,5,7-triazabicyclo(4.4.0)dec-5-ene, and 1,8-diazabicyclo[5.4.0]-undec-7-ene (DBU) had MBQ yields of 30, 38, and 59%, respectively. The most effective base was *N*,*N*-diisopropylethylamine (DIPEA), which afforded a 68% yield of MBQ.

We next sought to identify a correlation between pK_b of the base and MBQ yield. Surprisingly, we observed cases in which bases with both low and high pK_b values gave similar high yields (e.g., DIPEA and DBU) and bases with high pK_b values that gave significantly different yields (e.g., DBU and DBN). A lower bound on pK_b might exist for these reactions, as DABCO (pK_b = 8.4) failed to induce oxidation. In the absence of a correlation with basicity, we suggest that the structure of the bases may be more important. In addition, we do not expect that the addition of a base would reduce the energy of **7-TS**.

Aldehyde Formation. Quinones and aldehydes are often seen as co-products during the oxidations (Table 1). The calculated pathway for the oxidation of the lignin models to form benzaldehydes begins in the same way as the previous pathways. The inactive Co^{III}–hydroperoxide complex **4** is replaced with a second equivalent of the Co^{III}–superoxo adduct to form **16**. Transfer of a benzylic hydrogen from the phenol radical in **16** via **16-TS** results in the formation of **17**, which consists of a quinone methide and Co^{III}–hydroperoxide. Thus, the Co^{III}–hydroperoxo adduct is produced at two points in the aldehyde pathway, both of which must go through the energetically unfavorable **7-TS**. The quinone methide then undergoes tautomerization to form the benzaldehyde product.

In the absence of pyridine, exchange of the inactivated Co^{III}–hydroperoxo adduct in **4** with another equivalent of Co^{III}–superoxo adduct to form **16** is uphill energetically by 9.2, 5.5, and 3.7 kcal/mol for the S, G, and H models, respectively (Figure 6). For **16-TS,** the activation barriers

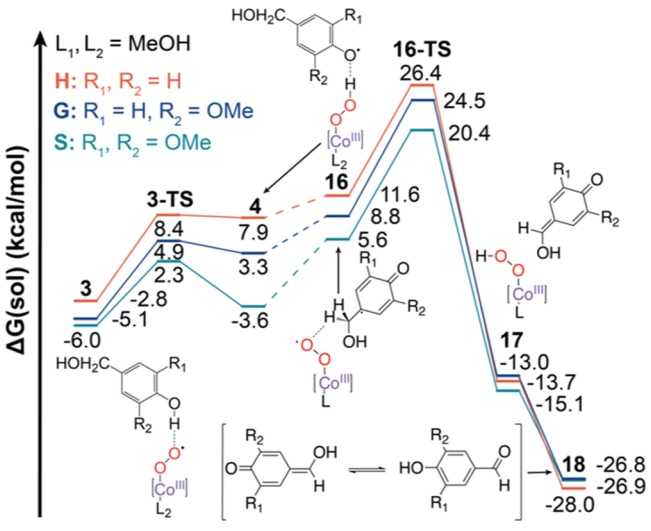

Figure 6. Free energy profile for the catalytic oxidation of lignin model compounds by Co(salen) without an axial pyridine ligand to form benzaldehydes. Energies are relative to **1**. Note that the inactivated Co^{III}–hydroperoxo species in **4** must be replaced by a second equivalent of the Co^{III}–superoxo complex to generate **16** and enable turnover. Dashed lines indicate the introduction of another equivalent of active catalyst.

follow the trend: G ≈ H > S, with free energies of 29.6, 29.2, and 26.4 kcal/mol, respectively, relative to **3**. From **17** to **18**, the free energy difference is 11.8–14.3 kcal/mol, indicating that there is a substantial thermodynamic driving force for syringaldehyde formation from the corresponding quinone methide intermediate.

https://dx.doi.org/10.1021/acssuschemeng.0c01970
ACS Sustainable Chem. Eng. XXXX, XXX, XXX–XXX

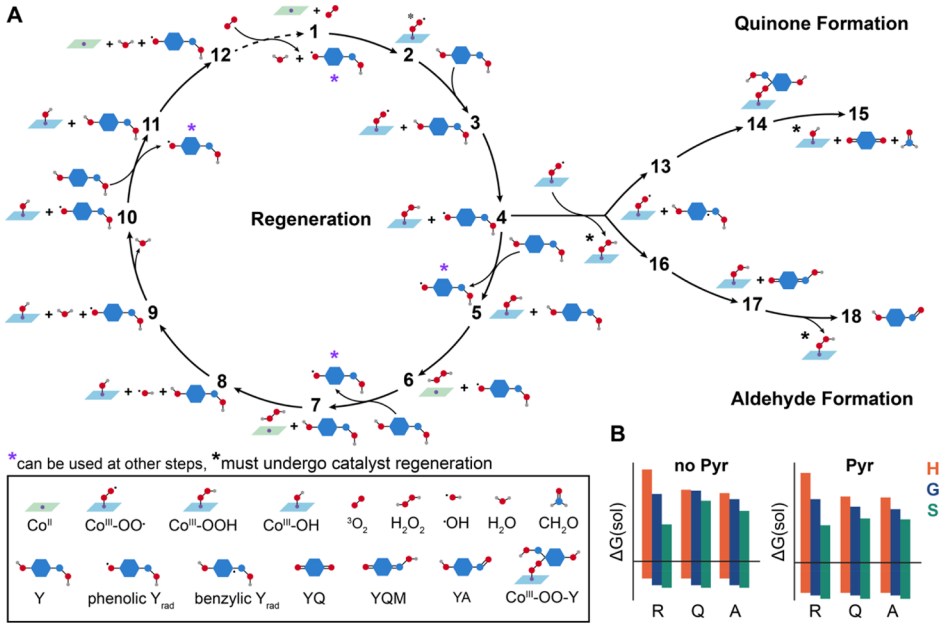

Figure 7. (A) Proposed mechanism for the formation of benzoquinones and benzaldehydes from lignin models. The lower-axial ligand to Co was omitted for simplicity. (B) Free energy differences (kcal/mol) between the lowest-energy intermediate and highest-energy transition state in each pathway (R = regeneration, Q = quinone formation, A = aldehyde formation).

The pyridine-free catalyst with the S lignin model gave a yield of 23% syringaldehyde after 1 h with a corresponding DMBQ yield for S of 36% (Table 1). Thus, the overall free energy barrier for DMBQ formation should be slightly lower than that for syringaldehyde. However, **14-TS** in DMBQ formation is higher in energy than **16-TS** in syringaldehyde formation (Figures 6 and S2).

We observed that reactions carried out with the S model for shorter times (i.e., 1 h) generated higher yields of aldehyde compared to longer reaction times. In the presence of 2,6-lutidine, oxidation of S for 1 h gave 26% aldehyde and 52% DMBQ (Table 1). Extending the reaction time to 22 h led to a slightly lower aldehyde yield (15%) and a minor increase in the yield of DMBQ (58%). Similar results were obtained in the absence of base, affording a syringaldehyde yield of 23% and a DMBQ yield of 36% after 1 h. After 22 h, the yield of syringaldehyde dropped to 8%, while that of DMBQ increased only slightly to 41%. These results indicate that syringaldehyde may be converted to DMBQ at longer reaction times. In our laboratory, we have found that these reactions proceed efficiently at room temperature but are less favorable at higher temperatures because oxygen is much less soluble in the latter case. Thus, we did not examine temperature effects further here.

Aldehydes as Intermediates in Quinone Formation. We next examined the possibility that aldehydes serve as a source of quinones by carrying out oxidations of three lignin model aldehydes under different conditions. In the absence of a coordinating base, syringaldehyde was converted to DMBQ with a yield of 26% after 1 h and 94% after 22 h (Table 3). However, neither vanillin nor 4-hydroxybenzaldehyde was converted to the corresponding quinone under any of the conditions tested (Table S1). Interestingly, a yield of only 3% was observed for this reaction with syringaldehyde in the presence of pyridine. This observation is consistent with early results,[34] where we observed that syringaldehyde was unique in that it failed to react in the presence of an external coordinating base but exhibited excellent oxidation otherwise. Our current working hypothesis is that syringaldehyde must first coordinate to the Co catalyst before undergoing oxidation. The presence of an external base blocks coordination sites on the Co, preventing oxidation.

Small amounts of aldehydes were generally observed in successful oxidations. Thus, we tested the oxidation of 3,4,5-trimethoxybenzyl alcohol to assess the formation of aldehydes through the removal of a benzylic hydrogen in a system lacking a phenolic hydrogen (Table 4). Under standard oxidation conditions, the yield of aldehyde remained low (<10%). Given that the aldehyde yield never exceeded the equivalency of catalyst, the catalyst appears to be sequestered after abstracting the benzylic hydrogen atom and is unable to achieve turnover. However, when the organic base was replaced with NaOH, oxidation occurred over longer reaction times (80 h). The primary oxidation product in this case was not the aldehyde but the corresponding carboxylic acid. Under these conditions, the aldehyde, which will show higher reactivity than the starting alcohol, undergoes further reaction to form the acid.

Mechanistic Cycle. The findings from this work enable construction of a mechanistic cycle in which intermediates can undergo exchange among the three pathways (Figure 7). Starting from **1**, both benzaldehyde and benzoquinone formation require two equivalents of a Co^{III}–superoxo adduct, the first of which is used to generate an H, G, or S radical, and the second is used to produce the corresponding product. The benzaldehyde pathway generates two equivalents of this intermediate per turnover, whereas the benzoquinone formation pathway generates a single Co^{III}–hydroperoxo adduct. Each inactive Co^{III}–hydroperoxo adduct must go through the complete regeneration pathway to sustain full catalytic activity, including through the energetically unfavorable **7-TS**. The phenolic radicals generated during the course of the regeneration pathway may be used at steps **13** or **16**, reducing the need to generate the Co^{III}–hydroperoxo adduct at **4**. In addition, the second equivalent of catalyst in

https://dx.doi.org/10.1021/acssuschemeng.0c01970
ACS Sustainable Chem. Eng. XXXX, XXX, XXX−XXX

benzoquinone formation used at step **13** is a Co^{III}–hydroxo adduct that can bypass **7-TS**. Thus, benzaldehyde formation may be more limited by regeneration bottlenecks than benzoquinone formation.

The mechanisms for regeneration of the Co^{III}–hydroxo and Co^{III}–hydroperoxo intermediates are consistent with previous proposals.[33,37] An important finding from the present work is that the inability of the H lignin model, 4-hydroxybenzyl alcohol, to facilitate catalyst regeneration explain the experimental observation that it failed to be converted to benzoquinone or benzaldehyde. The trend in free energy barriers for catalyst regeneration is H > G > S, which is consistent with experimental observations (Tables 1 and 2). For the H model, the energetic barrier for catalyst regeneration is substantially higher than for quinone and aldehyde formation. In contrast, for the S model alone, catalyst regeneration has a lower free energy barrier than both quinone and aldehyde formation and is therefore not a bottleneck for oxidation. The free energy barrier for catalyst regeneration with the G model is similar in magnitude to the corresponding quinone and aldehyde barriers.

CONCLUSIONS

Here, we have performed a complementary computational and experimental investigation of the mechanism of Co(salen)-catalyzed oxidation of monomeric H, G, and S lignin models to form benzoquinones and benzaldehydes. The identification of chemical and structural factors that limit catalytic efficiency of Co-Schiff base catalysts provided in this study is expected to lead to the development of improved catalysts. Our findings are consistent with previous work on Co(salen)-catalyzed oxidation of para-substituted phenols[33,34] and the addition of nitrogenous bases to improve oxidation.[32,47] The Co(salen) catalyst readily oxidizes the S lignin model when a pyridine ligand is present (99% DMBQ yield), and the calculated free energy barriers for catalyst regeneration and quinone or aldehyde formation are similar (24.9–27.4 kcal/mol), allowing for efficient turnover. However, no quinone formation was observed for the G and H lignin models, even upon addition of pyridine. For these systems, the calculated free energy barriers for catalyst regeneration were >30 kcal/mol, likely preventing sustained catalytic turnover. However, it was recently reported that quinones such as MBQ and BQ readily deactivate Co(salen) catalysts bearing a pyridine ligand.[38] Interestingly, oxidation of the G model was achieved by the addition of bulky, noncoordinating bases and resulted in MBQ yields of up to 68%.

The steric environment around the Co has been shown to have a notable effect on the reactivity of the catalyst.[49] Therefore, a viable strategy for enhancing the oxidation of G models includes further investigation into the use of sterically hindered nitrogenous bases (Table 2). Alternatively, bulky substituents could be added to the catalyst without requiring addition of an external axial ligand[38,49,50] Our working hypothesis is that noncoordinating bases enhance catalysis by deprotonating phenolic substrates to generate phenoxides, which are more easily oxidized to the phenoxy radical than a neutral phenol. In our estimation, the barrier for forming the phenoxy radical will be lowered but the barrier for catalyst regeneration is expected to remain the same in the presence of noncoordinating bases. Although we do not have hard evidence to support this argument, it is consistent with our observations. However, the addition of bulky substituents, sterically hindered nitrogenous bases, or other strong bases is not expected to lower the energetically unfavorable barrier for **7-TS** in the catalyst regeneration pathway. A potential alternative approach to catalytic oxidation of G and H lignin models would be to lower the overall free energy barrier for catalyst regeneration by incorporating a cocatalyst with favorable geometric and electronic features that promote O–O homolysis of the coordinated H_2O_2 intermediate.

ASSOCIATED CONTENT

Supporting Information

The Supporting Information is available free of charge at https://pubs.acs.org/doi/10.1021/acssuschemeng.0c01970.

Experimental and computational details and calculated energies (PDF)

Cartesian coordinates for all optimized geometries (ZIP)

AUTHOR INFORMATION

Corresponding Authors

Joseph J. Bozell – *Center for Renewable Carbon, University of Tennessee, Knoxville, Knoxville, Tennessee 37996, United States;* orcid.org/0000-0001-6952-963X; Email: jbozell@utk.edu

Jerry M. Parks – *Graduate School of Genome Science and Technology, University of Tennessee, Knoxville, Knoxville, Tennessee 37996, United States; Biosciences Division, Oak Ridge National Laboratory, Oak Ridge, Tennessee 37831, United States;* orcid.org/0000-0002-3103-9333; Email: parksjm@ornl.gov

Authors

Connor J. Cooper – *Graduate School of Genome Science and Technology, University of Tennessee, Knoxville, Knoxville, Tennessee 37996, United States; Biosciences Division, Oak Ridge National Laboratory, Oak Ridge, Tennessee 37831, United States;* orcid.org/0000-0002-5527-9948

Shahrina Alam – *Center for Renewable Carbon, University of Tennessee, Knoxville, Knoxville, Tennessee 37996, United States*

Vincent de Paul N. Nziko – *Biosciences Division, Oak Ridge National Laboratory, Oak Ridge, Tennessee 37831, United States*

Ryne C. Johnston – *Biosciences Division, Oak Ridge National Laboratory, Oak Ridge, Tennessee 37831, United States;* orcid.org/0000-0002-6606-9401

Alexander S. Ivanov – *Chemical Sciences Division, Oak Ridge National Laboratory, Oak Ridge, Tennessee 37831, United States*

Zhongyu Mou – *Biosciences Division, Oak Ridge National Laboratory, Oak Ridge, Tennessee 37831, United States*

David B. Turpin – *Alliance for Pulp and Paper Technology Innovation (APPTI), Washington, D.C. 20005, United States*

Alan W. Rudie – *USDA-Forest Service, Forest Products Laboratory, Madison, Wisconsin 53726, United States*

Thomas J. Elder – *USDA-Forest Service, Southern Research Station, Auburn, Alabama 36849, United States*

Complete contact information is available at: https://pubs.acs.org/10.1021/acssuschemeng.0c01970

Notes

The authors declare no competing financial interest.

https://dx.doi.org/10.1021/acssuschemeng.0c01970
ACS Sustainable Chem. Eng. XXXX, XXX, XXX–XXX

■ ACKNOWLEDGMENTS

This research was supported by the High-Performance Computing for Manufacturing Project Program (HPC4Mfg), which is managed by the U.S. Department of Energy (DOE) Advanced Manufacturing Office within the Energy Efficiency and Renewable Energy Office. This research used resources of the National Energy Research Scientific Computing Center (NERSC), a U.S. DOE Office of Science User Facility operated under Contract no. DE-AC02-05CH11231, and resources of the Compute and Data Environment for Science (CADES) at ORNL, which is managed by UT-Battelle, LLC for the U.S. DOE under Contract no. DE-AC05-00OR22725. C.J.C. was supported by a National Science Foundation Graduate Research Fellowship under Grant no. 2017219379.

■ REFERENCES

(1) Bozell, J. J. Feedstocks for the future - Biorefinery production of chemicals from renewable carbon. *Clean: Soil, Air, Water* **2008**, *36*, 641−647.
(2) Bozell, J. J.; Petersen, G. R. Technology development for the production of biobased products from biorefinery carbohydrates - the US Department of Energy's "Top 10" revisited. *Green Chem.* **2010**, *12*, 539−554.
(3) Bozell, J. J.; Holladay, J. E.; Johnson, D.; White, J. F. *Top Value-Added Chemicals from Biomass. Volume II—Results of Screening for Potential Candidates from Biorefinery Lignin*; United States. Department of Energy: Richland, WA, 2007.
(4) Zakzeski, J.; Bruijnincx, P. C. A.; Jongerius, A. L.; Weckhuysen, B. M. The catalytic valorization of lignin for the production of renewable chemicals. *Chem. Rev.* **2010**, *110*, 3552−3599.
(5) Sannigrahi, P.; Pu, Y.; Ragauskas, A. Cellulosic biorefineries-unleashing lignin opportunities. *Curr. Opin. Environ. Sust.* **2010**, *2*, 383−393.
(6) Ragauskas, A. J.; Beckham, G. T.; Biddy, M. J.; Chandra, R.; Chen, F.; Davis, M. F.; Davison, B. H.; Dixon, R. A.; Gilna, P.; Keller, M.; Langan, P.; Naskar, A. K.; Saddler, J. N.; Tschaplinski, T. J.; Tuskan, G. A.; Wyman, C. E. Lignin valorization: Improving lignin processing in the biorefinery. *Science* **2014**, *344*, 1246843.
(7) Lange, H.; Decina, S.; Crestini, C. Oxidative upgrade of lignin - Recent routes reviewed. *Eur. Polym. J.* **2013**, *49*, 1151−1173.
(8) Azadi, P.; Inderwildi, O. R.; Farnood, R.; King, D. A. Liquid fuels, hydrogen and chemicals from lignin: a critical review. *Renewable Sustainable Energy Rev.* **2013**, *21*, 506−523.
(9) Gasser, C. A.; Hommes, G.; Schäffer, A.; Corvini, P. F.-X. Multi-catalysis reactions: New prospects and challenges of biotechnology to valorize lignin. *Appl. Microbiol. Biotechnol.* **2012**, *95*, 1115−1134.
(10) Picart, P.; de María, P. D.; Schallmey, A. From gene to biorefinery: microbial β-etherases as promising biocatalysts for lignin valorization. *Front. Microbiol.* **2015**, *6*, 916.
(11) Laurichesse, S.; Avérous, L. Chemical modification of lignins: Towards biobased polymers. *Prog. Polym. Sci.* **2014**, *39*, 1266−1290.
(12) Li, C.; Zhao, X.; Wang, A.; Huber, G. W.; Zhang, T. Catalytic transformation of lignin for the production of chemicals and fuels. *Chem. Rev.* **2015**, *115*, 11559−11624.
(13) Chatel, G.; Rogers, R. D. Review: Oxidation of Lignin Using Ionic Liquids-An Innovative Strategy To Produce Renewable Chemicals. *ACS Sustainable Chem. Eng.* **2014**, *2*, 322−339.
(14) Bozell, J. J. Approaches to the selective catalytic conversion of lignin: a grand challenge for biorefinery development. *Top. Curr. Chem.* **2014**, *353*, 229−255.
(15) Boerjan, W.; Ralph, J.; Baucher, M. Ligninbiosynthesis. *Annu. Rev. Plant Biol.* **2003**, *54*, 519−546.
(16) Sangha, A. K.; Parks, J. M.; Standaert, R. F.; Ziebell, A.; Davis, M.; Smith, J. C. Radical coupling reactions in lignin synthesis: a density functional theory study. *J. Phys. Chem. B* **2012**, *116*, 4760−4768.
(17) Buranov, A. U.; Mazza, G. Lignin in straw of herbaceous crops. *Ind. Crops Prod.* **2008**, *28*, 237−259.
(18) Mosier, N.; Wyman, C.; Dale, B.; Elander, R.; Lee, Y. Y.; Holtzapple, M.; Ladisch, M. Features of promising technologies for pretreatment of lignocellulosic biomass. *Bioresour. Technol.* **2005**, *96*, 673−686.
(19) Key, R. E.; Bozell, J. J. Progress toward Lignin Valorization via Selective Catalytic Technologies and the Tailoring of Biosynthetic Pathways. *ACS Sustainable Chem. Eng.* **2016**, *4*, 5123−5135.
(20) Deuss, P. J.; Barta, K. From models to lignin: Transition metal catalysis for selective bond cleavage reactions. *Coord. Chem. Rev.* **2016**, *306*, 510−532.
(21) Díaz-Urrutia, C.; Chen, W.-C.; Crites, C.-O.; Daccache, J.; Korobkov, I.; Baker, R. T. Towards lignin valorisation: comparing homogeneous catalysts for the aerobic oxidation and depolymerisation of organosolv lignin. *RSC Adv.* **2015**, *5*, 70502−70511.
(22) Rinaldi, R.; Jastrzebski, R.; Clough, M. T.; Ralph, J.; Kennema, M.; Bruijnincx, P. C. A.; Weckhuysen, B. M. Paving the way for lignin valorisation: Recent advances in bioengineering, biorefining and catalysis. *Angew. Chem., Int. Ed.* **2016**, *55*, 8164−8215.
(23) Wu, A.; Patrick, B. O.; Chung, E.; James, B. R. Hydrogenolysis of β-O-4 lignin model dimers by a ruthenium-xantphos catalyst. *Dalton Trans.* **2012**, *41*, 11093−11106.
(24) Nichols, J. M.; Bishop, L. M.; Bergman, R. G.; Ellman, J. A. Catalytic C-O bond cleavage of 2-aryloxy-1-arylethanols and its application to the depolymerization of lignin-related polymers. *J. Am. Chem. Soc.* **2010**, *132*, 12554−12555.
(25) Sergeev, A. G.; Hartwig, J. F. Selective, nickel-catalyzed hydrogenolysis of aryl ethers. *Science* **2011**, *332*, 439−443.
(26) He, J.; Zhao, C.; Lercher, J. A. Ni-catalyzed cleavage of aryl ethers in the aqueous phase. *J. Am. Chem. Soc.* **2012**, *134*, 20768−20775.
(27) Parsell, T. H.; Owen, B. C.; Klein, I.; Jarrell, T. M.; Marcum, C. L.; Haupert, L. J.; Amundson, L. M.; Kenttämaa, H. I.; Ribeiro, F.; Miller, J. T.; Abu-Omar, M. M. Cleavage and hydrodeoxygenation (HDO) of C-O bonds relevant to lignin conversion using Pd/Zn synergistic catalysis. *Chem. Sci.* **2013**, *4*, 806−813.
(28) Hanson, S. K.; Wu, R.; Silks, L. A. P. C-C or C-O bond cleavage in a phenolic lignin model compound: selectivity depends on vanadium catalyst. *Angew. Chem., Int. Ed.* **2012**, *51*, 3410−3413.
(29) Son, S.; Toste, F. D. Non-oxidative vanadium-catalyzed C-O bond cleavage: application to degradation of lignin model compounds. *Angew. Chem., Int. Ed.* **2010**, *49*, 3791−3794.
(30) Rahimi, A.; Azarpira, A.; Kim, H.; Ralph, J.; Stahl, S. S. Chemoselective metal-free aerobic alcohol oxidation in lignin. *J. Am. Chem. Soc.* **2013**, *135*, 6415−6418.
(31) Biannic, B.; Bozell, J. J. Efficient cobalt-catalyzed oxidative conversion of lignin models to benzoquinones. *Org. Lett.* **2013**, *15*, 2730−2733.
(32) Cedeno, D.; Bozell, J. J. Catalytic oxidation of para-substituted phenols with cobalt-Schiff base complexes/O_2-selective conversion of syringyl and guaiacyl lignin models to benzoquinones. *Tetrahedron Lett.* **2012**, *53*, 2380−2383.
(33) Zombeck, A.; Drago, R. S.; Corden, B. B.; Gaul, J. H. Activation of molecular oxygen. Kinetic studies of the oxidation of hindered phenols with cobalt-dioxygen complexes. *J. Am. Chem. Soc.* **1981**, *103*, 7580−7585.
(34) Bozell, J. J.; Hames, B. R.; Dimmel, D. R. Cobalt-Schiff base complex catalyzed oxidation of para-substituted phenolics. Preparation of benzoquinones. *J. Org. Chem.* **1995**, *60*, 2398−2404.
(35) Kervinen, K.; Korpi, H.; Gerbrand Mesu, J.; Soulimani, F.; Repo, T.; Rieger, B.; Leskelä, M.; Weckhuysen, B. M. Mechanistic insights into the oxidation of veratryl alcohol with Co(salen) and oxygen in aqueous media: An in-situ spectroscopic study. *Eur. J. Inorg. Chem.* **2005**, *2005*, 2591−2599.
(36) Rajagopalan, B.; Cai, H.; Busch, D. H.; Subramaniam, B. The catalytic efficacy of Co(salen)(AL) in O_2 oxidation reactions in CO_2-expanded solvent media: axial ligand dependence and substrate selectivity. *Catal. Lett.* **2008**, *123*, 46−50.

https://dx.doi.org/10.1021/acssuschemeng.0c01970
ACS Sustainable Chem. Eng. XXXX, XXX, XXX−XXX

(37) Anson, C. W.; Ghosh, S.; Hammes-Schiffer, S.; Stahl, S. S. Co(salophen)-catalyzed aerobic oxidation of *p*-hydroquinone: Mechanism and implications for aerobic oxidation catalysis. *J. Am. Chem. Soc.* **2016**, *138*, 4186−4193.
(38) Zuleta, E. C.; Goenaga, G. A.; Zawodzinski, T. A.; Elder, T.; Bozell, J. J. Deactivation of Co-Schiff base catalysts in the oxidation of para-substituted lignin models for the production of benzoquinones. *Catal. Sci. Technol.* **2020**, *10*, 403−413.
(39) Zhao, Y.; Truhlar, D. G. A new local density functional for main-group thermochemistry, transition metal bonding, thermochemical kinetics, and noncovalent interactions. *J. Chem. Phys.* **2006**, *125*, 194101.
(40) Hay, P. J.; Wadt, W. R. Ab initio effective core potentials for molecular calculations. Potentials for the transition metal atoms Sc to Hg. *J. Chem. Phys.* **1985**, *82*, 270−283.
(41) Francl, M. M.; Pietro, W. J.; Hehre, W. J.; Binkley, J. S.; Gordon, M. S.; DeFrees, D. J.; Pople, J. A. Self-consistent molecular orbital methods. XXIII. A polarization-type basis set for second-row elements. *J. Chem. Phys.* **1982**, *77*, 3654−3665.
(42) Hehre, W. J.; Ditchfield, R.; Pople, J. A. Self-consistent molecular orbital methods. XII. Further extensions of Gaussian-type basis sets for use in molecular orbital studies of organic molecules. *J. Chem. Phys.* **1972**, *56*, 2257−2261.
(43) Hariharan, P. C.; Pople, J. A. The influence of polarization functions on molecular orbital hydrogenation energies. *Theor. Chim. Acta* **1973**, *28*, 213−222.
(44) Marenich, A. V.; Cramer, C. J.; Truhlar, D. G. Universal solvation model based on solute electron density and on a continuum model of the solvent defined by the bulk dielectric constant and atomic surface tensions. *J. Phys. Chem. B* **2009**, *113*, 6378−6396.
(45) Frisch, M. J.; Trucks, G. W.; Schlegel, H. B.; Scuseria, G. E.; Robb, M. A.; Cheeseman, J. R.; Scalmani, G.; Barone, V.; Petersson, G. A.; Nakatsuji, H.; Li, X.; Caricato, M.; Marenich, A. V.; Bloino, J.; Janesko, B. G.; Gomperts, R.; Mennucci, B.; Hratchian, H. P.; Ortiz, J. V.; Izmaylov, A. F.; Sonnenberg, J. L.; Williams; Ding, F.; Lipparini, F.; Egidi, F.; Goings, J.; Peng, B.; Petrone, A.; Henderson, T.; Ranasinghe, D.; Zakrzewski, V. G.; Gao, J.; Rega, N.; Zheng, G.; Liang, W.; Hada, M.; Ehara, M.; Toyota, K.; Fukuda, R.; Hasegawa, J.; Ishida, M.; Nakajima, T.; Honda, Y.; Kitao, O.; Nakai, H.; Vreven, T.; Throssell, K.; Montgomery, J. A., Jr.; Peralta, J. E.; Ogliaro, F.; Bearpark, M. J.; Heyd, J. J.; Brothers, E. N.; Kudin, K. N.; Staroverov, V. N.; Keith, T. A.; Kobayashi, R.; Normand, J.; Raghavachari, K.; Rendell, A. P.; Burant, J. C.; Iyengar, S. S.; Tomasi, J.; Cossi, M.; Millam, J. M.; Klene, M.; Adamo, C.; Cammi, R.; Ochterski, J. W.; Martin, R. L.; Morokuma, K.; Farkas, O.; Foresman, J. B.; Fox, D. J. *Gaussian 16*, Rev. A.03., Wallingford, CT, 2016.
(46) Samsel, E. G.; Kochi, J. K. Oxidative alkylation of cobalt complexes with hydrazines. *Inorg. Chem.* **1986**, *25*, 2450−2457.
(47) Elder, T.; Bozell, J. J.; Cedeno, D. The effect of axial ligand on the oxidation of syringyl alcohol by Co(salen) adducts. *Phys. Chem. Chem. Phys.* **2013**, *15*, 7328−7337.
(48) Howard, J. A.; Ingold, K. U. The inhibited autoxidation of styrene: Part II. The relative inhibiting efficiencies of meta- and para-substituted phenols. *Can. J. Chem.* **1963**, *41*, 1744−1751.
(49) Key, R. E.; Elder, T.; Bozell, J. J. Steric effects of bulky tethered arylpiperazines on the reactivity of Co-Schiff base oxidation catalysts-a synthetic and computational study. *Tetrahedron* **2019**, *75*, 3118−3127.
(50) Biannic, B.; Bozell, J. J.; Elder, T. Steric effects in the design of Co-Schiff base complexes for the catalytic oxidation of lignin models to para-benzoquinones. *Green Chem.* **2014**, *16*, 3635−3642.

https://dx.doi.org/10.1021/acssuschemeng.0c01970
ACS Sustainable Chem. Eng. XXXX, XXX, XXX−XXX